ACS APPLIED MATERIALS & INTERFACES

Research Article

www.acsami.org

Bifunctional Magnetic-Fluorescent Nanoparticles: Synthesis, Characterization, and Cell Imaging

Yanjiao Lu,[†] Yang Zheng,[‡] Shusen You,[†] Feng Wang,[†] Zhuo Gao,[†] Jie Shen,[‡] Wantai Yang,[†] and Meizhen Yin*[,†]

[†]State Key Laboratory of Chemical Resource Engineering, Key Laboratory of Carbon Fiber and Functional Polymers, Ministry of Education, Beijing Laboratory of Biomedical Materials, Beijing University of Chemical Technology, 100029 Beijing, China

[‡]Department of Entomology, China Agricultural University, 100193 Beijing, China

Supporting Information

ABSTRACT: A new type of bifunctional magnetic-fluorescent Fe_3O_4@SiO_2−PDI−PAA/Ca^{2+} nanoparticles has been prepared by coating PDI-cored star polymers (PDI−PAA) onto the surface of Fe_3O_4@SiO_2 core−shell nanostructures. The morphology and properties of the composite nanoparticles are investigated by transmission electron microscopy, ultraviolet−visible spectrometry, fluorescence spectrometry, and vibrating sample magnetometry. The composite nanoparticles display a strong red emission and superparamagnetic behavior at room temperature. The cell viability and uptake assays reveal good biocompatibility of these hybrid nanoparticles. Hence, the composite nanoparticles are of potential to be further explored as therapeutic vector in biomedical field.

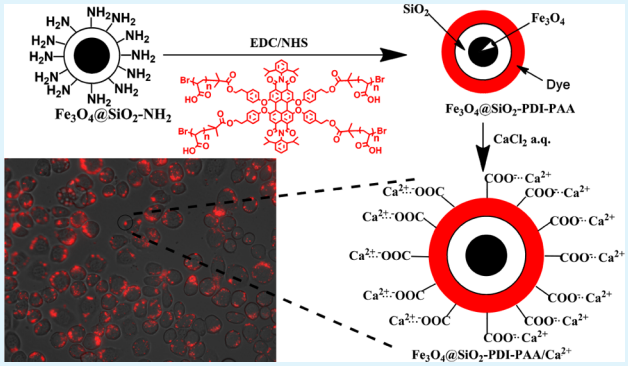

KEYWORDS: *star polymer, magnetic nanoparticles, fluorescence, bioimaging*

INTRODUCTION

In recent years, magnetic-fluorescent nanoparticles (NPs) have been extensively investigated because of their improved physical and chemical properties.[1,2] The bifunctional NPs allow not only multimodal imaging (e.g., magnetic resonance and fluorescence imaging), but also intracellular movements to be controlled in a magnetic field with real-time monitoring using fluorescent microscopy. Because superparamagnetic NPs have already been applied to cell separation,[3] magnetic resonance imaging (MRI) contrast agents,[4,5] magnetically assisted drug delivery,[6] mediators for hyperthermic cancer treatment,[7] and DNA sensor.[8] The magnetic and fluorescent materials will open up great prospects in biomedical applications.[9−11]

There is a great need for the development of these bifunctional nanocomposites, but there are some difficulties to be overcome in their fabrication such as the fluorescence quenching problem. The resolution is providing a stable shell[12,13] or an appropriate spacer between the magnetic core and fluorescent molecules.[14,15] For a shell coating of an NP, silica provides an effective barrier to prevent the fluorescence quenching via controlling the thickness.[1] In addition, silica has been widely used to protect the core of the NPs from the external environment, thereby improving the stability of the NPs.[16,17] Another important aspect is that silica is highly biocompatible and its surface can be easily modified with amines, thiols, or carboxyl groups, which enables covalent modification of the particle surface for biological applications.[18]

Perylene diimide (PDI) derivatives have been widely used in many fields, such as organic solar cell,[19] chemical sensor,[20] and biomedicine[21] because of their outstanding thermal, chemical, and photoelectron stability.[22] Previously, core−shell PDI-cored star polymers with water-solubility and biocompatibility have been synthesized and used as bioimaging agents and gene carriers.[23−26] In addition, the core−shell PDI-cored star polymers can be fluorescently excited in a long wavelength, i.e. in the visible or near-infrared range. It is favorable to deep tissue penetration for in vivo imaging. Most importantly, the core−shell PDI-cored star polymers provide a sufficiently long spacer to bypass any possible quenching by the paramagnetic core.

In this paper, we report the simple and fast synthesis of Fe_3O_4@SiO_2−PDI−PAA/Ca^{2+} NPs with good magnetic and fluorescent properties together. The PDI-cored star polymer (PDI−PAA) was prepared through atom transfer radical polymerization (ATRP) strategy. The Fe_3O_4 NPs synthesized by the facile chemical coprecipitation method were encapsulated with SiO_2 via the reverse microemulsion method and further coated by PDI−PAA. To increase the rate of positive-

Received: November 25, 2014
Accepted: February 18, 2015
Published: February 18, 2015

DOI: 10.1021/am508266p
ACS Appl. Mater. Interfaces 2015, 7, 5226−5232

charge-facilitated cell endocytosis, the obtained Fe_3O_4@SiO_2−PDI−PAA NPs were complexed with calcium ion.[27−29] The stability, cytotoxicity, and cellular uptake of such NPs were investigated for potential biomedical applications, such as drug delivery and magnetic imaging.

EXPERIMENTAL SECTION

Materials. Ferric chloride hexahydrate ($FeCl_3·6H_2O$, Tianjin Fuchen Chemical Reagent Factory) and ferrous sulfate heptahydrate ($FeSO_4·7H_2O$, Xilong Chemical Co., Ltd.), oleic acid (OA, Tianjin Fuchen Chemical Reagent Factory), *N*-hydroxysuccinimide (NHS, Alfa Aesar) and N-(3-(dimethylamino)propyl)-N′-ethylcarbodiimide (EDC, Alfa Aesar) were used as purchased without further purification. Sodium chloride, (3-aminopropyl) triethoxysilane (APTES), tetraethyl orthosilicate (TEOS), cyclohexane, hexanol, ethanol, disodium hydrogen phosphate (Na_2HPO_4), sodium dihydrogen phosphate (NaH_2PO_4), ninhydrin, calcium chloride, and ammonia aqueous solutions (25%) were purchased from Beijing Chemical Plant and were used directly. *N,N′*-Bis(2,6-diisopropylphenyl)-1,6,7,12-tetra[4-(ethyl-2-bromoisobutyrate)phenoxy]perylene-3,4,9,10-tetracarboxylic acid diimide (PDI-4Br)[30] was synthesized as previous report. *Tert*-butyl acrylate (*t*BA, Alfa Aesar, 99%) was purified by vacuum distillation before use. Triethylamine (TEA, Alfa Aesar, 99%) was stirred with KOH overnight at room temperature, refluxed with CaH_2, and distilled before use. Other reagents were purchased from Alfa Aesar without further purification.

Synthesis of PDI−PAA. *Synthesis of PDI-PtBA.* A Schlenk tube was charged with the initiator PDI-4Br (50 mg, 0.027 mmol, 1 equiv), CuBr (15.3 mg, 0.108 mmol, 4 × 1 equiv) and tBA (1.39 g, 10.9 mmol, 400 equiv). They were dissolved by dry 2-butanone (2.0 mL) absolutely. After three freeze−pump−thaw cycles, DTB-bipy (15 mg, 0.216 mmol, 4 × 2 equiv) was added and the tube was sealed in N_2 atmosphere. To ensure the catalyst completely formed complex, the solution was stirred for 10 min. The polymerization was carried out at 90 °C. After 10 h, the solution was dissolved in dichloromethane and passed an alumina column to eliminate the used copper salt. Then it was precipitated in methanol/water mixture (v/v = 1:1, 3 × 50 mL). After drying in vacuum for 12 h at room temperature, PDI-P*t*BA was obtained as a red powder.

Hydrolysis of PDI-PtBA. A Schlenk flask was charged with the polymer PDI-P*t*BA (200 mg). To eliminate the air, the flask was flushed with N_2 gas flow for 10 min. Dichloromethane (20 mL) was added and the polymer was completely dissolved. Then, trifluoroacetic acid (TFA, 10 mL) was added, and the red solution was stirred at room temperature for 24 h. After that, the solvent in the resulting cloudy mixture was removed by rotary evaporation, and the residual solid was washed with dichloromethane three times. After drying the solution under a vacuum at room temperature for 10 h, PDI−PAA was obtained as a red solid.

Synthesis of Magnetic-Fluorescent NPs. *Synthesis of Fe_3O_4 NPs.* The preparation of OA-coated MNPs was performed according to a literature-based method:[31] 2.35 g of $FeSO_4·7H_2O$ and 4.1 g of $FeCl_3·6H_2O$ were dissolved into 100 mL of deionized water in a flask. This solution was stirred for 30 min under N_2 flow, followed by adding 25 mL of ammonia aqueous solutions (25%) quickly at room temperature. The solution color changed from orange to black, leading to a black precipitate. Then under vigorous stirring, 1 mL of OA was dropped into the dispersion slowly at 80 °C in 1 h. The mixture was allowed to react another 1 h under nitrogen atmosphere. After cooled to room temperature, small amount of sodium chloride was added into the system. Then, the above solution and cyclohexane were mixed together in an extractor to extract Fe_3O_4 NPs from water into cyclohexane. Under the protection of single layer of OA, the Fe_3O_4 NPs had good dispersibility in cyclohexane. Finally, the cyclohexane dispersion was evaporated under reduced pressure to remove the solvent and then the residual was dried in a vacuum for 12 h to give rise to as black power.

Synthesis of Fe_3O_4@SiO_2 NPs. The Fe_3O_4@SiO_2 core−shell NPs were synthesized according to a reverse microemulsion method.[32] Typically, 6 mg of dried Fe_3O_4 NPs were dissolved in 38 mL of cyclohexane and then 10 g of triton X-100, 8 mL of hexanol, and 1.7 mL of H_2O were added under ultrasonication at room temperature. Subsequently, 0.2 mL TEOS was added to the above mixture solution. After 4 h of stirring, 0.6 mL of ammonia aqueous solutions (25%) was introduced dropwise to initiate the TEOS hydrolysis and the reaction was continued to proceed at room temperature for 24 h under constant mechanical stirring. Ethanol was added to the solution to form dark precipitates, which were collected through magnetic separation. The dark precipitates were further purified by ultrasonication in ethanol for several times to remove surfactant and unreacted reactants. They were dried under a vacuum for 12 h.

Synthesis of Fe_3O_4@SiO_2−NH_2 NPs. Amine-functionalized Fe_3O_4@SiO_2 microspheres were prepared using 3-aminopropyltriethoxysilane (APTES) according to the reported method with some modifications.[33] 10 mg of Fe_3O_4@SiO_2 NPs were dispersed in the mixture of ethanol (20 mL) and water (4 mL) under ultrasonication and a mechanical stirring. Subsequently, 0.48 mL of ammonium aqueous solutions (25%) and 0.4 mL of APTES were added to above solution and the mixture was stirred for 24 h at room temperature. The NPs were centrifuged from the solution, washed with ethanol five times, and then dried in a vacuum for 10 h.

Synthesis of Fe_3O_4@SiO_2−PDI−PAA NPs. Briefly, 1 mg of PDI−PAA, 10 mg of EDC, and 12 mg of NHS were dissolved in phosphate buffer solution (0.2 mol/L Na_2HPO_4−NaH_2PO_4, 30 mL, pH 6.0). Ten mg of the above prepared Fe_3O_4@SiO_2 NPs were added into the buffer mixture under ultrasonication at 0 °C for 10 min and then the mixture was warmed to room temperature. The mixed solution was stirred for an additional 24 h at room temperature. Finally, the NPs were separated from the solution through centrifugation, washed with deionized water, and then dried in a vacuum for 10 h.

Synthesis of Fe_3O_4@SiO_2−PDI−PAA/Ca^{2+} NPs. Ten milligrams of Fe_3O_4@SiO_2−PDI−PAA NPs were dispersed in deionized water and then added into gently stirred $CaCl_2$ solution (3%, w/v). After being stirred for 24 h, the NPs were separated from the solution through centrifugation, washed with deionized water five times to remove unreacted $CaCl_2$, saved in refrigerator for the following biological applications.

Cytotoxicity Test and Cellular Uptake. The cytotoxicity test and cellular uptake experiments were performed according to the procedure described in our previous work.[32]

Characterization. The proton nuclear magnetic resonance (^{1}H NMR) spectra were performed on the "'Bruker-Spectrospin"' instrument (400 MHz) at room temperature. Gel Permeation Chromatography (GPC) chromatograms were conducted with a Waters 515 pump and Waters 410 differential refractometer using PSS columns in THF as an eluent at 30 °C at a flow rate of 1 mL/min, calibrated with linear PSt standards. Mass spectra (MS) were measured with a XEVO-G2QTOF (ESI) (Waters, USA). UV−visible spectra were obtained on a spectrometer (Cintra 20, GBC, Australia). The corrected fluorescence spectroscopic studies were performed on a fluorescence spectrophotometer (Horiba Jobin Yvon FluoroMax-4 NIR, NJ, USA) at room temperature (25 °C). Morphology of NPs was observed with a JEOL JEM-3010 high resolution transmission electron microscope (HRTEM) manipulated at an accelerating voltage of 200 kV. Samples were prepared by placing a drop of the as-synthesized NPs dispersion in ethanol on a clean copper grid, and then evaporating at ambient temperature. Powder X-ray diffraction (XRD) patterns were recorded on a D/max2500 VB2+/PC X-ray diffractometer (Rigaku) using Cu Kα radiation in the 2θ range 5−90°. X-ray Zeta-potential measurements were carried out on a Brookhaven 90 Plus/BI-MAS particle size analyzer with ultrasonically redispersed particles in water at 25 °C. Magnetic characterization was carried out on a vibrating sample magnetometer (VSM, Jilin University JDM-13 VSM) at room temperature. X-ray photoelectron spectroscopy (XPS) analyses of dried powder samples were conducted on an ESCALAB 250 apparatus with an AlKa radiation source, at 9×10^{-9} mmHg of analysis chamber pressure. All binding energies were referenced to C 1s peak at 284.6 eV.

DOI: 10.1021/am508266p
ACS Appl. Mater. Interfaces 2015, 7, 5226−5232

Scheme 1. Synthesis of PDI−PAA

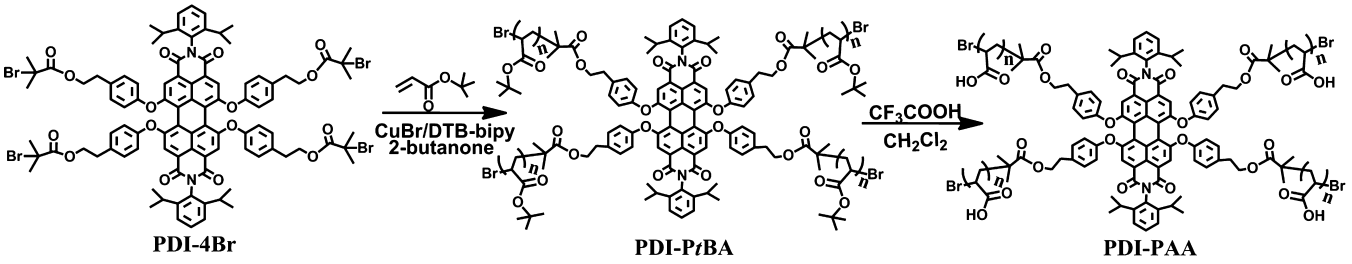

RESULTS AND DISCUSSION

Synthesis of Fluorescent Star Polymer (PDI−PAA) and Magnetic-Fluorescent Fe_3O_4@SiO_2−PDI−PAA/Ca^{2+} NPs.

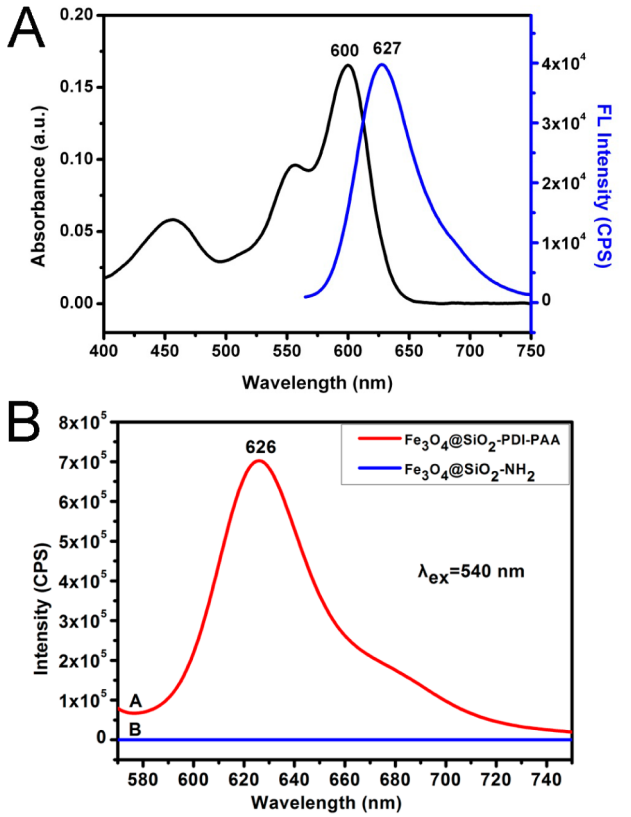

Figure 1. (A) UV absorption and emission spectra of PDI−PAA; (B) fluorescent emission spectra of Fe_3O_4@SiO_2−PDI−PAA NPs (red) and Fe_3O_4@SiO_2−NH_2 NPs (blue).

The PDI-cored star polymer (PDI−PAA) with carboxylic groups was prepared through ATRP strategy indirectly by a previously reported method (Scheme 1). The detailed descriptions can be found in the Experimental Section. First, PDI-4Br was synthesized as the ATRP initiator according to the reference.[29] Then, PDI-P*t*BA was synthesized via ATRP (Figure S1 in the Supporting Information) and the removal of the *tert*-butyl protective groups was achieved under acidic conditions to yield the target polymer PDI−PAA (Figure S2 in the Supporting Information). The repeat units of each arm in PDI−PAA were well controlled to about 50, determined by ^{1}H NMR and GPC (Table S1 in the Supporting Information). The absorption and fluorescence spectra of PDI−PAA in water are shown in Figure 1A. Upon excitation at 540 nm, the PDI−PAA exhibits a broad band emission centered at 627 nm, which is beneficial for biological imaging experiments with less autofluorescence background. It is known that carboxylic groups can complex with calcium ion by electrostatic interactions.[27−29] Then the Fe_3O_4@SiO_2−PDI−PAA/Ca^{2+} NPs with good magnetic and fluorescent properties were designed and prepared. The synthesis procedure is schematically illustrated in Scheme 2, such as the synthesis of Fe_3O_4 NPs, encapsulation of Fe_3O_4 NPs in SiO_2 shells, modification of silica surface with $-NH_2$ groups, coating PDI−PAA onto the surface of silica, and complexion with calcium ion.

Fe_3O_4 NPs were synthesized by coprecipitation method with OA as the surfactant. The crystal structure of the NPs was determined by XRD (Figure S3 in the Supporting Information). All detected diffraction peaks [(1 1 1), (2 2 0), (3 1 1), (4 0 0), (4 2 2), (5 1 1), and (4 4 0)] were consistent with that of the structure of Fe_3O_4 (JCPDS card No. 19−0629). Fe_3O_4@SiO_2 core−shell structures were prepared using a reverse microemulsion method.

To attach covalently PDI−PAA on the outer surface of silica shell, we further treated Fe_3O_4@SiO_2 NPs with APTES, which reacted with the surface silanol groups to produce silica surface functionalized with $-NH_2$ groups. As shown in Figure S4 in the Supporting Information, the functionalization with amine groups was proved by the chromogenic reaction with ninhydrin.[34] The color of the solution shows slight yellow as original (Figure S4A in the Supporting Information), and the color turned blue when the NPs were modified with amine groups (Figure S4B in the Supporting Information). PDI−PAA was easily coated onto the surface of Fe_3O_4@SiO_2 core−shell nanostructures via the reaction between $-NH_2$ and $-COOH$. To confirm the successful grafting of PDI−PAA, the Fe_3O_4@SiO_2−PDI−PAA NPs were dispersed in water at room temperature for fluorescence measurement. The emission maximum was recorded at 626 nm (Figure 1B), which is the characteristic emission of PDI−PAA (Figure 1A). The fluorescence quantum yield of the nanocomplex was 13.1% at room temperature using the compound 4[35] in water (Φ_f = 66%) as a reference.

Finally, the Fe_3O_4@SiO_2−PDI−PAA NPs were complexed with calcium ion by mixing the NPs with $CaCl_2$ solution. The successful complex of Ca^{2+} on the NPs was characterized by XPS (Figure 2). As the Fe_3O_4 core disturbs XPS signal, the SiO_2−PDI−PAA/Ca^{2+} NPs used for XPS measurement was also prepared. Compared to the SiO_2−PDI−PAA NPs (Figure 2B), the SiO_2−PDI−PAA/Ca^{2+} NPs (Figure 2A) showed obvious increase of the Ca peak, which indicated the successful complex of Ca^{2+} on the NPs. This process leads to the formation of Fe_3O_4@SiO_2−PDI−PAA/Ca^{2+} NPs. The Fe_3O_4@SiO_2−PDI−PAA/Ca^{2+} NPs have the same emission peak (626 nm) when dispersed in water at room temperature (Figure S5 in the Supporting Information).

DOI: 10.1021/am508266p
ACS Appl. Mater. Interfaces 2015, 7, 5226−5232

Scheme 2. Schematic Representation of the Formation of Fe_3O_4@SiO_2−PDI−PAA/Ca^{2+} NPs

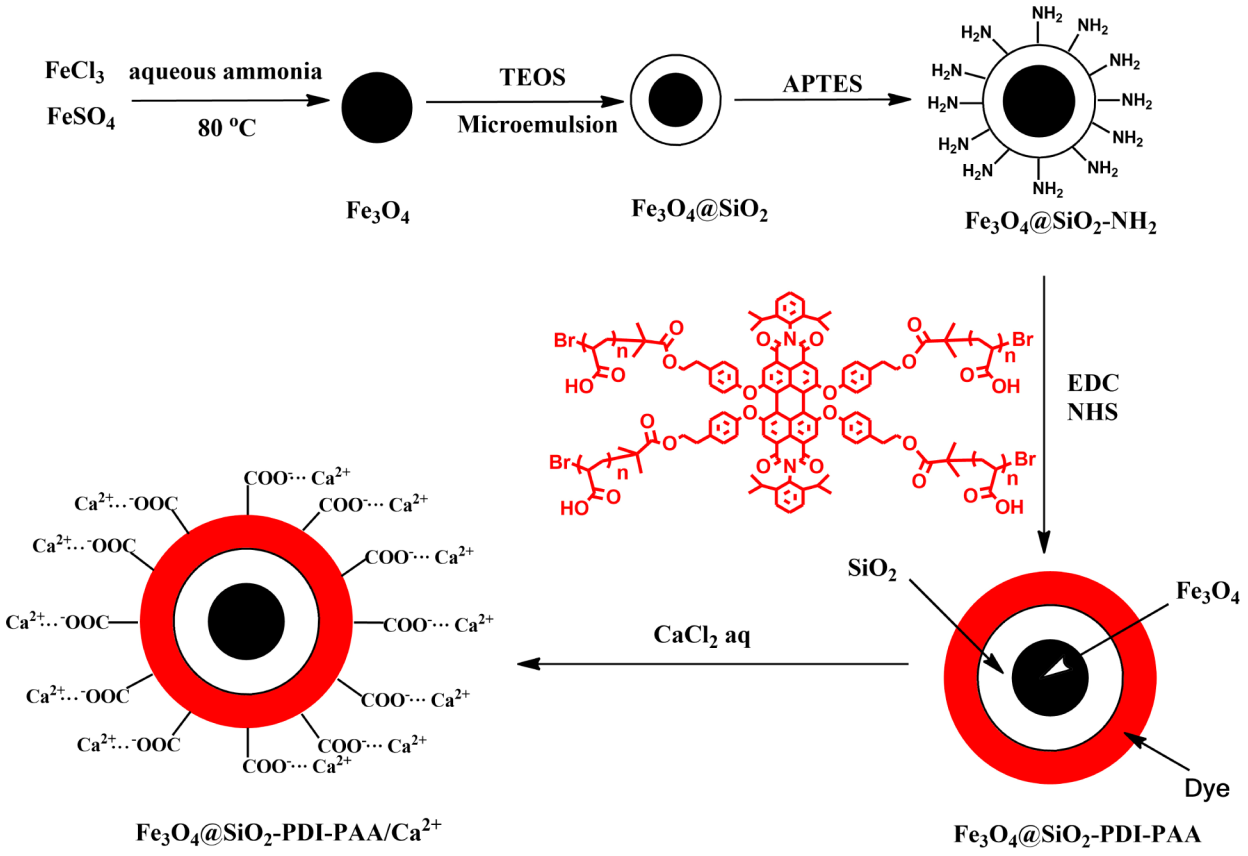

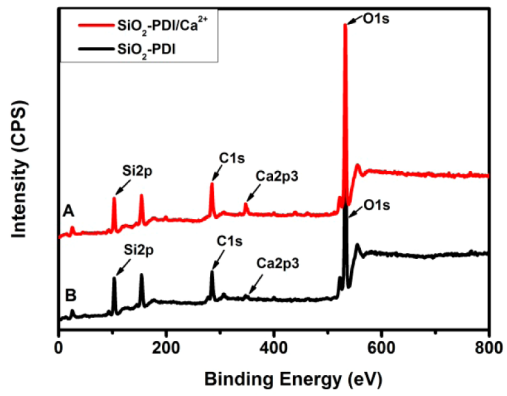

Figure 2. XPS pattern of (A) SiO_2−PDI−PAA/Ca^{2+} NPs and (B) SiO_2−PDI−PAA NPs.

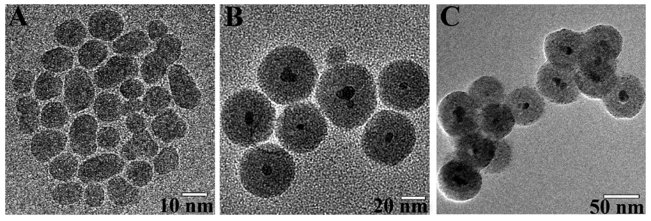

Figure 3. TEM images of the (A) Fe_3O_4, (B) Fe_3O_4 @SiO_2, and (C) Fe_3O_4@SiO_2−PDI−PAA/Ca^{2+} NPs.

Morphologies of the NPs. The morphologies of the prepared products were characterized by high resolution transmission electron microscopy (HRTEM). Figure 3 shows

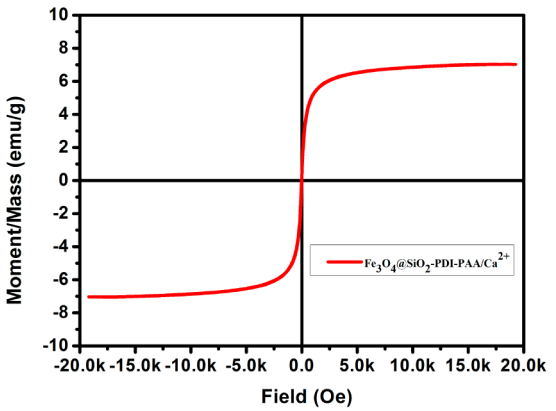

Figure 4. Hysteresis loop of the Fe_3O_4@SiO_2−PDI−PAA/Ca^{2+} NPs.

the typical TEM images of Fe_3O_4 NPs, Fe_3O_4@SiO_2 core−shell NPs, and final Fe_3O_4@SiO_2−PDI−PAA/Ca^{2+} NPs. Their size distributions were performed by using the Nano Measurer (Figure S6 in the Supporting Information).

Fe_3O_4 NPs are 10 nm in diameter. One Fe_3O_4 NP was encapsulated by the silica shell layer with an approximate thickness of 20 nm. The monodispersed Fe_3O_4@SiO_2 NPs have nearly spherical core−shell structures. The final Fe_3O_4@SiO_2−PDI−PAA/Ca^{2+} NPs have an average diameter of 60 nm and a rough outer surface. It is also found that the resulted Fe_3O_4@SiO_2−PDI−PAA/Ca^{2+} NPs can be easily dispersed in an aqueous solution.

Magnetic Property of the Fe_3O_4@SiO_2−PDI−PAA/Ca^{2+} NPs. To investigate the magnetic property of the Fe_3O_4@SiO_2−PDI−PAA/Ca^{2+} NPs, we measured the magnetization

DOI: 10.1021/am508266p
ACS Appl. Mater. Interfaces 2015, 7, 5226−5232

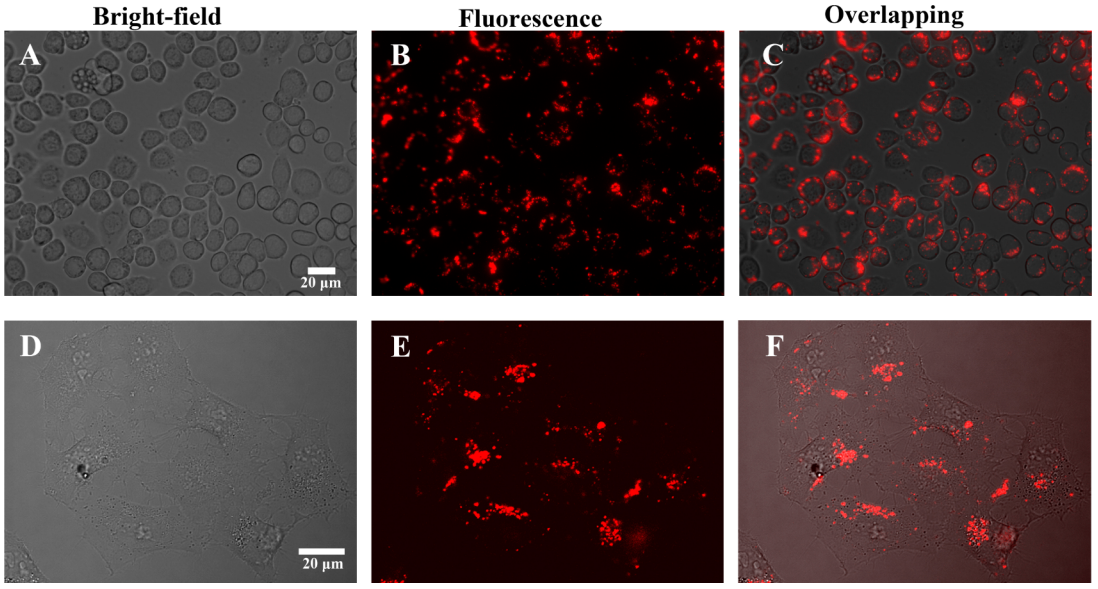

Figure 5. Fluorescence images of (A–C) SF9 and (D–F) Hela cells incubated with Fe_3O_4@SiO_2–PDI–PAA/Ca^{2+} NPs for 10 h. (A, D) Bright-field, (B, E) fluorescence, and (C, F) overlapping images.

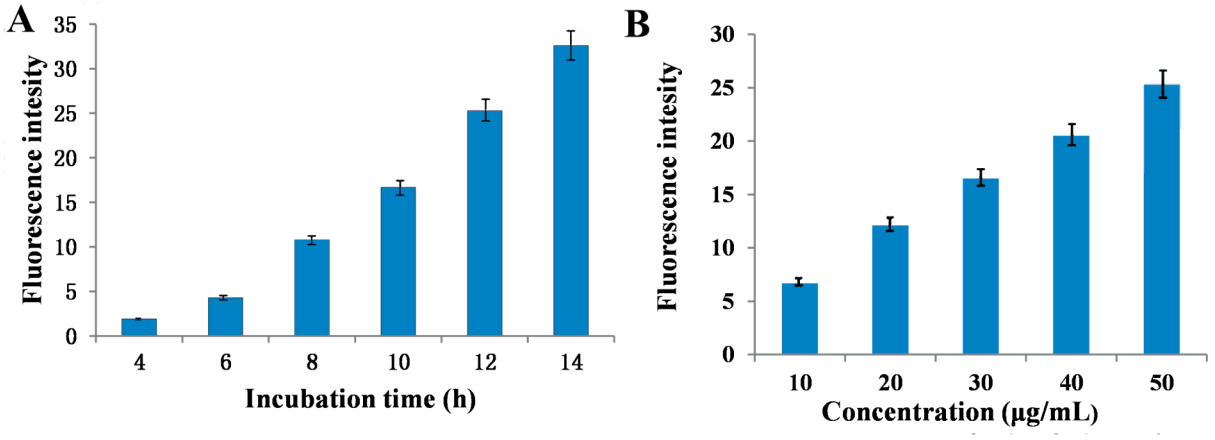

Figure 6. Quantified fluorescence intensities of cellular distributed NPs. (A) Cells were treated with 40 μg/mL Fe_3O_4@SiO_2–PDI–PAA/Ca^{2+} NPs for different incubation time. (B) Cells were treated with various concentrations of NPs for 12 h.

curves on VSM with the magnetic field cycle between −20 and +20 kOe. As shown in Figure 4, the composite NPs exhibited a superparamagnetic behavior with a specific saturation magnetization of 7.04 emu g^{-1} because of the presence of Fe_3O_4 in the nanocomposite. Although the saturation magnetization is much lower than Fe_3O_4 NPs' (Figure S7 in the Supporting Information), the Fe_3O_4@SiO_2–PDI–PAA/Ca^{2+} NPs can be separated rapidly by magnet (Figure S8 in the Supporting Information).

Cytotoxicity of the Fe_3O_4@SiO_2–PDI–PAA/Ca^{2+} NPs. Biocompatibility is a critical issue for nanomaterial's biomedical applications. To verify the biocompatibility of these magnetic-fluorescent NPs, cell viability upon exposure to Fe_3O_4@SiO_2–PDI–PAA/Ca^{2+} NPs was measured by a Tali cell viability assay. Figure S9 in the Supporting Information shows the concentration effect of the Fe_3O_4@SiO_2–PDI–PAA/Ca^{2+} NPs with 48 h incubation on cell viability.

The results clearly indicate that the cell viability remains as high as 93% even at a high concentration of NPs (0.1 mg mL^{-1}). The low cytotoxicity of the NPs demonstrates that the Fe_3O_4@SiO_2–PDI–PAA/Ca^{2+} NPs fulfill the requirements of potential biological applications.

Cellular Uptake. To investigate the ability of the Fe_3O_4@SiO_2–PDI–PAA/Ca^{2+} NPs to enter live cells, we carried out cellular uptake experiments using *Spodoptera frugiperda* 9 (SF9) and Hela cells. After 10 h incubation with the NPs at 37 °C, the cells were examined by fluorescence microscopy to observe cellular distribution of the NPs (Figure 5). The NPs can be internalized into cells and light up the cells. To quantify the effects of incubation time and concentration, we measured the fluorescence intensities of cellular NPs, which showed a gradual increase in the cells along with incubation time (Figure 6 A) and NP concentration (Figure 6B). These data suggest that the Fe_3O_4@SiO_2–PDI–PAA/Ca^{2+} NPs have good capacity for cell's internalization.

CONCLUSIONS

In summary, a facile method for synthesis of bifunctional magnetic-fluorescent core–shell NPs was reported. Briefly, PDI-cored star polymer (PDI–PAA) was synthesized through ATRP strategy. The Fe_3O_4@SiO_2–PDI–PAA/Ca^{2+} NPs were

DOI: 10.1021/am508266p
ACS Appl. Mater. Interfaces 2015, 7, 5226–5232

successfully synthesized by coating PDI−PAA onto the Fe_3O_4@SiO_2 NPs and then complexed with calcium ion by electrostatic adherence. These water-soluble hybrid nanocomposites retain the magnetic property of Fe_3O_4 and good fluorescence stability. In vitro experiments clearly confirmed that these Fe_3O_4@SiO_2−PDI−PAA/Ca^{2+} NPs have low cytotoxicity and high intracellular penetration. The bifunctional NPs have much potential to be applied in various biomedical applications, such as drug delivery and optical and magnetic imaging.

■ ASSOCIATED CONTENT

Supporting Information

Characterization of the polymers and supporting table and figures. The material is available free of charge via the Internet at http://pubs.acs.org.

■ AUTHOR INFORMATION

Corresponding Author

*E-mail: yinmz@mail.buct.edu.cn.

Notes

The authors declare no competing financial interest.

■ ACKNOWLEDGMENTS

The work was financially supported by the National Natural Science Foundation of China (21174012, 51103008, and 51221002), the Doctoral Program of Higher Education Research Fund (20120010110008), and the Beijing Natural Science Foundation (2142026).

■ REFERENCES

(1) Corr, S. A.; Rakovich, Y. P.; Gun'ko, Y. K. Multifunctional Magnetic-Fluorescent Nanocomposites for Biomedical Applications. *Nanoscale Res. Lett.* **2008**, *3*, 87−104.

(2) Zhang, X.; Zhang, X.; Yang, B.; Yang, Y.; Wei, Y. Renewable Itaconic Acid Based Cross-Linked Fluorescent Polymeric Nanoparticles for Cell Imaging. *Polym. Chem.* **2014**, *20*, 5885−5889.

(3) Yoon, T. J.; Yu, K. N.; Kim, E.; Kim, J. S.; Kim, B. G.; Yun, S. H.; Sohn, B. H.; Cho, M. H.; Lee, J. K.; Park, S. B. Specific Targeting, Cell Sorting, and Bioimaging with Smart Magnetic Silica Core-Shell Nanomaterials. *Small* **2006**, *2*, 209−215.

(4) Sabareesh, K. Fluorescent and Paramagnetic Core-Shell Hybrid Nanoparticles for Bi-Modal Magnetic Resonance/Luminescence Imaging. *J. Mater. Chem.* **2012**, *22*, 20641−20648.

(5) Hsu, B. Y. W.; Wang, M.; Zhang, Y.; Vijayaragavan, V.; Wong, S. Y.; Chang, A. Y.-C.; Bhakoo, K. K.; Li, X.; Wang, J. Silica-F127 Nanohybrid-Encapsulated Manganese Oxide Nanoparticles for Optimized T1Magnetic Resonance Relaxivity. *Nanoscale* **2014**, *6*, 293−299.

(6) Chen, Y.; Chen, H.; Zeng, D.; Tian, Y.; Chen, F.; Feng, J.; Shi, J. Core/Shell Structured Hollow Mesoporous Nanocapsules: A Potential Platform for Simultaneous Cell Imaging and Anticancer Drug Delivery. *ACS Nano* **2010**, *4*, 6001−6013.

(7) Jordan, A.; Scholz, R.; Maier-Hauff, K.; Johannsen, M.; Wust, P.; Nadobny, J.; Schirra, H.; Schmidt, H.; Deger, S.; Loening, S. Presentation of a New Magnetic Field Therapy System for the Treatment of Human Solid Tumors with Magnetic Fluid Hyperthermia. *J. Magn. Magn. Mater.* **2001**, *225*, 118−126.

(8) Kouassi, G. K.; Irudayaraj, J. Magnetic and Gold-Coated Magnetic Nanoparticles as a DNA Sensor. *Anal. Chem.* **2006**, *78*, 3234−3241.

(9) Gao, J.; Zhang, W.; Huang, P.; Zhang, B.; Zhang, X.; Xu, B. Intracellular Spatial Control of Fluorescent Magnetic Nanoparticles. *J. Am. Chem. Soc.* **2008**, *130*, 3710−3711.

(10) Sahu, S.; Mohapatra, S. Multifunctional Magnetic Fluorescent Hybrid Nanoparticles as Carriers for the Hydrophobic Anticancer Drug 5-Fluorouracil. *Dalton Trans.* **2013**, *42*, 2224−2231.

(11) Zhang, X.; Zhang, X.; Tao, L.; Chi, Z.; Xu, J.; Wei, Y. Aggregation Induced Emission-Based Fluorescent Nanoparticles: Fabrication Methodologies and Biomedical Applications. *J. Mater. Chem. B* **2014**, *28*, 4398−4414.

(12) Gong, X.; Zhang, Q.; Cui, Y.; Zhu, S.; Su, W.; Yang, Q.; Chang, J. A Facile Method to Prepare High-Performance Magnetic and Fluorescent Bifunctional Nanocomposites and Their Preliminary Application in Biomolecule Detection. *J. Mater. Chem. B* **2013**, *1*, 2098−2106.

(13) Tong, L.; Shi, J.; Liu, D.; Li, Q.; Ren, X.; Yang, H. Luminescent and Magnetic Properties of Fe_3O_4@SiO_2@Y_2O_3: Eu^{3+} Composites with Core−Shell Structure. *J. Phys. Chem. C* **2012**, *116*, 7153−7157.

(14) Huh, Y.-M.; Jun, Y.-w.; Song, H.-T.; Kim, S.; Choi, J.-s.; Lee, J.-H.; Yoon, S.; Kim, K.-S.; Shin, J.-S.; Suh, J.-S. In Vivo Magnetic Resonance Detection of Cancer by Using Multifunctional Magnetic Nanocrystals. *J. Am. Chem. Soc.* **2005**, *127*, 12387−12391.

(15) Gu, H.; Xu, K.; Yang, Z.; Chang, C. K.; Xu, B. Synthesis and Cellular Uptake of Porphyrin Decorated Iron Oxide Nanoparticles-a Potential Candidate for Bimodal Anticancer Therapy. *Chem. Commun.* **2005**, 4270−4272.

(16) Lee, C. S.; Chang, H. H.; Bae, P. K.; Jung, J.; Chung, B. H. Bifunctional Nanoparticles Constructed Using One-Pot Encapsulation of a Fluorescent Polymer and Magnetic (Fe_3O_4) Nanoparticles in a Silica Shell. *Macromol. Biosci.* **2012**, *13*, 321−331.

(17) Zhang, Y.; Wang, M.; Zheng, Y.-g.; Tan, H.; Hsu, B. Y.-w.; Yang, Z.-c.; Wong, S. Y.; Chang, A. Y.-c.; Choolani, M.; Li, X. Peolated Micelle/Silica as Dual-Layer Protection of Quantum Dots for Stable and Targeted Bioimaging. *Chem. Mater.* **2013**, *25*, 2976−2985.

(18) Yang, H.; Zhuang, Y.; Hu, H.; Du, X.; Zhang, C.; Shi, X.; Wu, H.; Yang, S. Silica-Coated Manganese Oxide Nanoparticles as a Platform for Targeted Magnetic Resonance and Fluorescence Imaging of Cancer Cells. *Adv. Funct. Mater.* **2010**, *20*, 1733−1741.

(19) Schmidt-Mende, L.; Fechtenkötter, A.; Müllen, K.; Moons, E.; Friend, R.; MacKenzie, J. Self-Organized Discotic Liquid Crystals for High-Efficiency Organic Photovoltaics. *Science* **2001**, *293*, 1119−1122.

(20) Zhou, R.; Li, B.; Wu, N.; Gao, G.; You, J.; Lan, J. Cyclen-Functionalized Perylenebisimides as Sensitive and Selective Fluorescent Sensors for Pb^{2+} in Aqueous Solution. *Chem. Commun.* **2011**, *47*, 6668−6670.

(21) Yin, M.; Shen, J.; Pflugfelder, G. O.; Müllen, K. A Fluorescent Core-Shell Dendritic Macromolecule Specifically Stains the Extracellular Matrix. *J. Am. Chem. Soc.* **2008**, *130*, 7806−7807.

(22) Kaiser, T. E.; Stepanenko, V.; Würthner, F. Fluorescent J-Aggregates of Core-Substituted Perylene Bisimides: Studies on Structure-Property Relationship, Nucleation-Elongation Mechanism, and Sergeants-and-Soldiers Principle. *J. Am. Chem. Soc.* **2009**, *131*, 6719−6732.

(23) Xu, Z.; He, B.; Shen, J.; Yang, W.; Yin, M. Fluorescent Water-Soluble Perylenediimide-Cored Cationic Dendrimers: Synthesis, Optical Properties, and Cell Uptake. *Chem. Commun.* **2013**, *49*, 3646−3648.

(24) Yin, M.; Shen, J.; Gropeanu, R.; Pflugfelder, G. O.; Weil, T.; Müllen, K. Fluorescent Core/Shell Nanoparticles for Specific Cell-Nucleus Staining. *Small* **2008**, *4*, 894−898.

(25) Yin, M.; Feng, C.; Shen, J.; Yu, Y.; Xu, Z.; Yang, W.; Knoll, W.; Müllen, K. Dual-Responsive Interaction to Detect DNA on Template-Based Fluorescent Nanotubes. *Small* **2011**, *7*, 1629−1634.

(26) Li, J.; Guo, K.; Shen, J.; Yang, W.; Yin, M. A Difunctional Squarylium Indocyanine Dye Distinguishes Dead Cells through Diverse Staining of the Cell Nuclei/Membranes. *Small* **2014**, *10*, 1351−1360.

(27) Alhakamy, N. A.; Berkland, C. J. Polyarginine Molecular Weight Determines Transfection Efficiency of Calcium Condensed Complexes. *Mol. Pharmacol.* **2013**, *10*, 1940−1948.

DOI: 10.1021/am508266p
ACS Appl. Mater. Interfaces 2015, 7, 5226−5232

(28) Cui, J.; Wang, M.; Zheng, Y.; Rodríguez Muñiz, G. M.; del Campo, A. n. Light-Triggered Cross-Linking of Alginates with Caged Ca^{2+}. *Biomacromolecules* **2013**, *14*, 1251−1256.
(29) Gujarathi, N. A.; Rane, B. R.; Patel, J. K. Ph Sensitive Polyelectrolyte Complex of O-Carboxymethyl Chitosan and Poly (Acrylic Acid) Cross-Linked with Calcium for Sustained Delivery of Acid Susceptible Drugs. *Int. J. Pharm.* **2012**, *436*, 418−425.
(30) Klok, H. A.; Becker, S.; Schuch, F.; Pakula, T.; Müllen, K. Fluorescent Star-Shaped Polystyrenes: ″Core-First″ Synthesis from Perylene-Based ATRP Initiators and Dynamic Mechanical Solid-State Properties. *Macromol. Chem. Phys.* **2002**, *203*, 1106−1113.
(31) Sun, Y.; Ding, X.; Zheng, Z.; Cheng, X.; Hu, X.; Peng, Y. Surface Initiated ATRP in the Synthesis of Iron Oxide/Polystyrene Core/Shell Nanoparticles. *Eur. Polym. J.* **2007**, *43*, 762−772.
(32) Lu, Y.; He, B.; Shen, J.; Li, J.; Yang, W.; Yin, M. Multifunctional Magnetic and Fluorescent Core−Shell Nanoparticles for Bioimaging. *Nanoscale* **2015**, *7*, 1606−1609.
(33) Zhang, Y.; Pan, S.; Teng, X.; Luo, Y.; Li, G. Bifunctional Magnetic-Luminescent Nanocomposites: Y_2O_3/Tb Nanorods on the Surface of Iron Oxide/Silica Core-Shell Nanostructures. *J. Phys. Chem. C* **2008**, *112*, 9623−9626.
(34) Yemm, E.; Cocking, E.; Ricketts, R. The Determination of Amino-Acids with Ninhydrin. *Analyst* **1955**, *80*, 209−214.
(35) Peneva, K.; Mihov, G.; Nolde, F.; Rocha, S.; Hotta, J. i.; Braeckmans, K.; Hofkens, J.; Uji-i, H.; Herrmann, A.; Müllen, K. Water-Soluble Monofunctional Perylene and Terrylene Dyes: Powerful Labels for Single-Enzyme Tracking. *Angew. Chem., Int. Ed.* **2008**, *120*, 3420−3423.

DOI: 10.1021/am508266p
ACS Appl. Mater. Interfaces 2015, 7, 5226−5232